/ Materials Science and Engineering C 75 (2017) 1006–1013

Contents lists available at ScienceDirect

Materials Science and Engineering C

journal homepage: www.elsevier.com/locate/msec

Alkali-etching growth of nest-like Ag@mTiO$_2$ hierarchical nanostructures and their potential applications

Zongnan Zhang [a], Haijiao Zhang [a,b,*]

[a] Institute of Nanochemistry and Nanobiology, School of Environmental and Chemical Engineering, Shanghai University, Shanghai 200444, PR China
[b] State Key Laboratory of Molecular Engineering of Polymers, Department of Macromolecular Science, Fudan University, Shanghai 200433, PR China

ARTICLE INFO

Article history:
Received 25 July 2016
Received in revised form 21 December 2016
Accepted 2 March 2017
Available online 03 March 2017

Keywords:
Ag@mTiO$_2$
Nest-like
Nanostructure
Alkali-etching
Drug carrier

ABSTRACT

Porous nanomaterials have attracted extensive interests in adsorption, catalysis, biosensors, and biomedicine due to their high surface area, well-defined pore structure and tunable pore size. However, how to obtain porous nanomaterials of desirable component and unique structure with multifunctionalities and synergetic properties is still a great challenge. In this work, a novel nest-like Ag@mTiO$_2$ hierarchical nanostructure with Ag nanoparticle as the core and a mesoporous crystalline TiO$_2$ as the protective shell was successfully prepared by layer-by-layer assembly technique and alkali-etching hydrothermal route. By simply changing the conditions of alkali etching, different nanostructures could be obtained, such as core-shell or rattle type. In the process, the thickness of coating silica layer and TiO$_2$ shell both played important roles for the formation of desired nanostructures. The as-prepared products had a large specific surface area of 301 m^2/g and a tailored TiO$_2$ outer shell. Raman spectra results showed perfect SERS signal of the tags enhanced and remained good stability even after one month. Doxycycline (Doxy) was chosen to evaluate their drug loading and controlled release properties. The results indicated that the obtained Ag@mTiO$_2$ nanoparticles exhibited good biocompatibility and excellent drug-loading capacity. Consequently, they are also expected to serve as ideal candidates for more potential applications including photocatalysis, drug controlled release, biosensor and cell imaging, etc.

1. Introduction

Since the discovery of MCM-41 in 1992 by Mobil [1], mesoporous materials have attracted extensive interest in many fields such as adsorption, catalysis, sensors and biomedicine due to their high specific surface area, adjustable pore size, tailored pore structure and controlled morphology, etc. [2–5] Up to now, significant progress has been made to prepare the mesoporous materials with various morphologies and nanostructures to expand their more applications. However, the application of traditional porous materials with single component was hindered owing to their limited functionality. Consequently, many efforts have been devoted to rationally design of core-shell, hollow or yolk-shell nanostructures with functional interior core and useful outer porous shell [6–16]. In these materials, the functional nanoparticles (NPs) as the core usually contain Au NPs [17,18], quantum dots (QDs) [19,20],or Fe_3O_4 magnetic NPs, etc. [21,22] On the other hand, functional outer shells can be achieved through appropriate chemical tailoring, for example, well-known layer-by-layer (LBL) method [23]. As a result, the core-shell nanostructures not only own the function of a single component, but also more interesting properties. For the reason, core-shell nanostructures have recently been subject to extensive research for their unique characteristics including high surface area, low density, and potential applications in various fields [24–29]. So far, numerous approaches based on the template-assisted process [30,31], Kirkendall effect [32,33], Ostwald ripening [34,35], and surfactant-involved strategy [36] have been developed to fabricate special core-shell structures. Especially, it should be mentioned that silica-etching technique has been regarded as an effective route to obtain various core-shell or rattle-type nanostructures through a facile etching process. In general, the etching agents such as NaOH, aqueous ammonia solution, Na_2CO_3 are widely used, as well as HF. Compared with toxic and corrosive HF, the basic reagents are relatively mild, safe, and easily tunable. Hence, constructing novel and hybrid nanostructures by a facile silica-etching method is still important. In addition, since great progress has been achieved for fabrication of porous core-shell or yolk-shell structure by using Ag as core, which is usually composed of anisotropic building blocks regarding one-dimensional (1D) nanowire, nanotube, and 2D nanosheet [37–39]. Therefore, it remains a great challenge to develop a new strategy for fabricating the desired hierarchical nanostructures with a Ag core and a functionally mesoporous shell with expected synergetic properties, especially some unique shell structures.

* Corresponding author at: Institute of Nanochemistry and Nanobiology, School of Environmental and Chemical Engineering, Shanghai University, Shanghai 200444, PR China.
E-mail address: hjzhang128@shu.edu.cn (H. Zhang).

http://dx.doi.org/10.1016/j.msec.2017.03.018
0928-4931/

Herein, a novel nest-like Ag@mTiO_2 hierarchical nanostructure with Ag nanoparticle as the core and a mesoporous crystalline TiO_2 as the protective shell was prepared starting from tetrabutyl titanate (TBOT) and tetraethyl orthosilicate (TEOS) by an alkali-etching hydrothermal assisted crystallization. In this case, the coated TiO_2 shell greatly enhanced the stability of the surface enhanced Raman scattering (SERS) signal of the tags to meet the potential application of bioimaging. In the meanwhile, the TiO_2 porous shells effectively reduced the possible cytotoxicity of Ag NPs owing to the oxidative effect in living cells [40]. Moverover, Ag@mTiO_2 nanostructure with a porous shell and a high surface area could make it as a promising candidate as drug carrier.

2. Experimental

2.1. Materials

All chemicals were of analytical grade and used without further purification. Tetraethoxysilane (TEOS) (99.9%), tetrabutyl titanate (TBOT), polyvinylpyrrolidone (PVP, Mw = 55.000), aqueous ammonia solution ($NH_3 \cdot H_2O$, 25–28 wt%), sodium hydroxide (NaOH), sodium carbonate (Na_2CO_3), $AgNO_3$, NH_4NO_3, ethanol, ethylene glycol, acetone, which were supplied by Sinopharm Chemical Reagent Co., Ltd. Doxycycline (Doxy, 99.9%) was purchased from Beijing Huafeng United Technology Co., Ltd. Cell Counting Kit-8 (CCK-8) was purchased from Dojindo Molecular Technologies (Japan). For cell culture medium, Dulbecco's Modified Eagle's Medium (DMEM), fetal bovine serum and glutamine were obtained from Invitrogen (USA), penicillin/streptomycin was purchased from GIBCO (USA). Mesenchymal stemcells (MSC) were provided by Dr. Lu Zhang from Shanghai Jiao Tong University. Deionized water was used in all experiments.

2.2. Synthesis of Ag nanoparticles

The Ag nanoparticles (NPs) were synthesized via a modified method, as reported by Xia et al [41]. Typically, 2.5 g of PVP (Mw = 55.000) was dissolved in 200 mL of ethylene glycol before 1.0 g of $AgNO_3$ was added. After a three-neck flask was set in an oil bath, the mixture was then heated to 130 °C within 30 min under vigorous stirring and maintained at 130 °C for 1 h to obtain the Ag nanoparticles. The Ag NPs were isolated by precipitating the solution with acetone (300–800 mL), followed by centrifugation at 10000 rpm for 3 min, and re-dispersed in 40 mL of ethanol to obtain 0.02 g/mL Ag NPs solution.

2.3. Synthesis of Ag@SiO_2 core-shell nanoparticles

The Ag@SiO_2 nanoparticles with different thickness of silica layer were prepared according to a typical Stöber method. In a typical procedure for the silica layer coating with the thickness of ~30 nm, 10 mL of Ag NPs/ethanol solution (0.02 g/mL) obtained above was dispersed in the mixture of ethanol (130 mL) and water (20 mL) and 2.5 mL of aqueous ammonia solution (28 wt%), then 1000 μL of TEOS was added dropwise in above solution under stirring. The reaction was continued for 12 h. The Ag@SiO_2 nanoparticles were separated by centrifugation and washed by ethanol and water for several times. The thickness of the silica layer could be readily controlled by changing the TEOS amounts. For example, silica coating layer with the thickness of ~50 nm was obtained using the procedure similar to the above increasing the TEOS concentration to 2000 μL.

2.4. Synthesis of Ag@SiO_2@TiO_2 core-shell nanoparticles

The core-shell Ag@SiO_2@TiO_2 nanoparticles were synthesized based on the hydrolysis and condensation of TBOT. Typically, the above obtained Ag@SiO_2 NPs (0.15 g) were dispersed in 200 mL of ethanol and mixed with 0.9 mL of aqueous ammonia solution (25–28 wt%) by ultrasonication for 15 min. Afterwards, 1000 μL of TBOT was added dropwise within 5 min, and the reaction was allowed to proceed at 45 °C for 24 h under stirring. The resultant product was separated by centrifugation and washed with deionized water and ethanol for 3 times, respectively. Similarly, the thickness of the TiO_2 layer could also be adjusted by altering the TBOT amounts. For example, TiO_2 layer with the thickness of ~50 nm was obtained using the procedure similar to the above increasing the TBOT concentration to 2000 μL.

2.5. Synthesis of nest-like and yolk-shell structured Ag@mTiO_2 nanoparticles

The Ag@mTiO_2 NPs were synthesized through using a kind of alkaline aqueous solution with different concentration as the etching agent such as NaOH, aqueous ammonia solution, Na_2CO_3. Typically, the above obtained Ag@SiO_2@TiO_2 (0.5 g) were mixed with an aqueous alkaline solution of NaOH (20 mL, 1.0 M), then added into a Teflon-lined stainless-steel autoclave at 150 °C for 24 h. After reaction, the products were immersed in HCl solutions (100 mL, 0.1 M) for 20 min and subsequently washed with deionized water until pH value was close to 7, and then dried at 60 °C. Finally, the nest-like Ag@mTiO_2 nanoparticles were obtained.

Especially, when using the aqueous ammonia solution as the alkaline etching agent under similar conditions, the morphologies have obviously changed and the yolk-shell structured Ag@mTiO_2 nanoparticles were got. Additionally, it should be mentioned that the yolk-shell structured Ag@mTiO_2 nanoparticles were also prepared under different condition. For example, the as-prepared Ag@SiO_2@TiO_2 were mixed with an aqueous alkaline solution of Na_2CO_3 (0.5 M) at 80 °C for 3 h. To further explore the formation mechanism of the Ag@mTiO_2 nanoparticles, a series of products were also prepared by varying the precursor compositions and reaction time.

2.6. Cell viability test

Mesenchymal stem cells (MSC) were grown in Dulbecco's Modified Eagle's Medium (DMEM) supplemented with 10% heat inactivated fetal bovine serum, 2 mM glutamine and 100 IU/mL penicillin and 100 μg/mL streptomycin in a humidified incubator with 5% CO_2 at 37 °C. The morphology of cells was observed by using an optical microscopy (Leica, Germany).

The cell viability in the presence of Ag@mTiO_2 nanoparticles was evaluated using the cell counting kit-8 (CCK-8) assay. MSC were seeded into 96-well plates at a density of $1 * 10^4$ per well in 100 mL of media and grown overnight. The cells were then incubated at various concentrations of nest-like Ag@mTiO_2 nanoparticles (5, 15, 25, and 50 μg/mL) for 12 h and 24 h, respectively. Following the incubation, cells were washed with D-Hanks buffer solution and incubated in100 μL fresh cell culture medium containing 10 μL CCK-8 solution (5 mg/mL) for 4 h. Thereafter, the CCK-8 solution was removed and the precipitated violet crystals were dissolved in 100 μL of DMSO. The absorbance in cell test was measured at 450 nm using a microplate reader (Bio-TEK instrument, Inc). The following formula was used to calculate the viability of cell growth: Viability (%) = (mean of absorbance value of treatment group / mean absorbance value of control) × 100. The results were expressed as an average over six identical measurements of each time point.

2.7. Loading and in vitro release of doxycycline (Doxy)

The doxycycline (Doxy) solutions with various concentrations were obtained by dissolving the given amounts of drug in PBS (pH = 7.4) solutions. In a typical experiment, 10 mg of nest-like Ag@mTiO_2 nanoparticles was dispersed in 10 mL of Doxy solution with various initial concentrations, and stirred at 25 °C for 24 h to achieve equilibrium. The equilibrium concentration of Doxy was determined by UV–Vis

spectrophotometer at the maximum absorbance of 272 nm. The following formula was used to calculate the loading rate:

Loading rate (%) = 100% × (Total amount of Doxy − Free Doxy in solution) / Total amount of Ag@mTiO$_2$ nanoparticles.

The Doxy release was performed by immersing 5 mg of Doxy-loaded Ag@mTiO$_2$ particles in dialysis bag containing 6 mL of PBS solution (pH = 7.4). Then, the dialysis bag was placed in a beaker filled with 200 mL of PBS solution (pH = 7.4), keeping stirring at 37 °C. Afterwards, the samples were removed at a given time interval and an equal amount of the same medium was supplied to maintain a constant volume. The amount of released drug was measured by a UV–Vis spectrophotometer at 272 nm.

2.8. Characterizations

The properties and morphology of samples were studied by transmission electron microscopy (TEM, JEOL 200CX), scanning electron microscopy (SEM, JEOL JSM-6700F), High resolution transmission electron microscopy (HRTEM, JSM-2010F). Elemental qualitative analysis was conducted by the energy-dispersive X-ray spectroscopy (EDX, OXFORD INCA) which was mounted in the JSM-6700F. X-ray powder diffraction (XRD) patterns were obtained on the Japan Rigakul D/max-2550 instrument operating at 40 kV and 40 mA using CuKα radiation (λ = 0.154 nm). Raman spectra were measured with Renishaw inVia Raman microscope using 514 nm lasers as a light source. N_2 adsorption-desorption isotherms were recorded on a QUADRASORB SI surface area & pore size analyzer at 77 K, after the product were annealed at 120 °C for 6 h. The Brunauer-Emmett-Teller (BET) specific surface area was calculated by using adsorption data. UV–Vis absorption spectra were recorded on a HITACHI U-3010 UV–Vis spectrophotometer.

3. Results and discussion

3.1. Structure and morphology

A typical schematic representation for the formation process of Ag@mTiO$_2$ hierarchical nanostructure is illustrated in Scheme 1. The total process was mainly divided into four parts. Firstly, Ag NPs was synthesized according to the previous method [41]. Then, the silica layer was coated onto the surface of Ag NPs according to a typical Stöber method. Subsequently, TiO_2 was explored to uniformly coat the SiO_2 layer by the hydrolysis and condensation of TBOT, giving rise to a typical sandwich structure (Ag@SiO$_2$@TiO$_2$). Finally, the desired hierarchical nanostructures were obtained through the hydrothermal alkali treatment process when the thickness of TiO_2 layer was suitable. During the process, the SiO_2 layer coated Ag NPs in the second step played the role of the media and template, which could be controlled from 10 to 50 nm by simply changing the amount of TEOS in the precursor (Fig. S1). Similarly, the shell thickness of TiO_2 layer was also a very important parameter, which directly decided the formation of the desired nanostructures (Fig. S2). More significantly, the structure and morphology of the final products could be well-tailored by accurately adjusting the reaction time, the strength and types of alkali sources, such as nest-like and rattle-type nanostructure (Scheme 1 and Fig. S3).

The morphology evolution of the products was observed by TEM technique. Fig. 1 shows the TEM images of the products at different stages. As was observed, the Ag NPs obtained were well-dispersed with an average diameter of 60 nm (Fig. 1A), followed by coating the silica layer with a thickness of 30 nm (Fig. 1B). After that, the uniform TiO_2 layer was further deposited onto the surface of silica layer, and the thickness was about 30 nm, in which the sandwich-like Ag@SiO$_2$@TiO$_2$ nanostructure was obtained (Fig. 1C). By close observation, the Ag@SiO$_2$@TiO$_2$ NPs possessed relatively rough surface compared with Ag@SiO$_2$ NPs, which may be attributed to the fact that the hydrolysis and condensation of TBOT was clearly faster than TEOS. TEM images (Fig. S2) further confirm the rough surface and the typical sandwich structure. At the end, the target product was successfully formed after the hydrothermal treatment in NaOH solution (1.0 M) at 150 °C. The Ag@mTiO$_2$ NPs showed the unique nest-like hierarchical nanostructures with an average size of 200 nm (Fig. 1D and Fig. S2E), and the outer shell was built by numberous thin TiO_2 nanosheets.

Fig. 2a shows the HRTEM image of the product. That further confirmed that Ag@mTiO$_2$ was composed of a compact core and a lower density porous shell, in accordance with the above TEM result. The SAED pattern and magnified TEM image (inset in Fig. 2a) indicated the crystalline nature of TiO_2 shell. STEM image clearly revealed that the Ag@mTiO$_2$ was constructed by the Ag core and TiO_2 porous shell (Fig. 2b and Fig. 2c). Elemental mapping analysis (Fig. 2d–f) combining with the EDX spectrum of the nanoparticles (Fig. 2g) also showed the presence of Ag, Ti and O elements, indicating their high purity, while a small amounts of Na and Si elements derived from the residue after the hydrothermal treatment in NaOH system, in line with the results reported by Zhao et al [37].

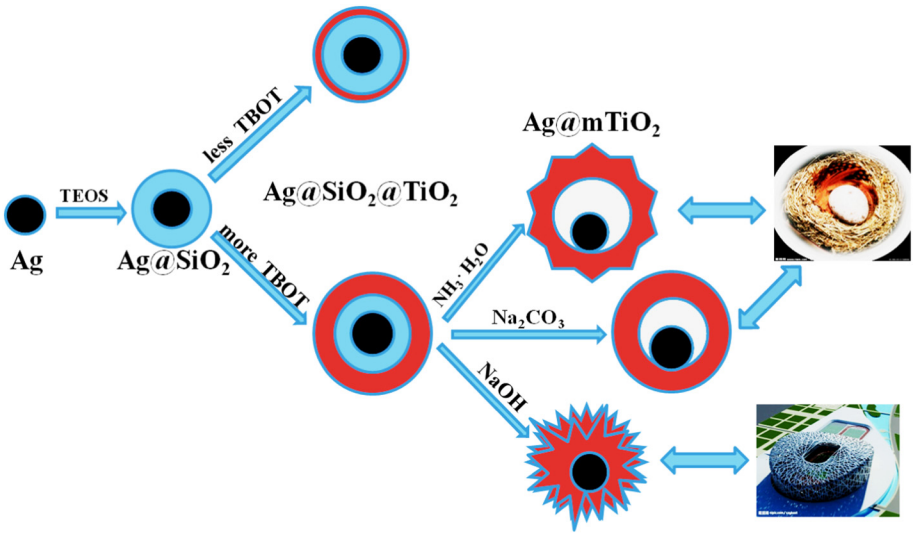

Scheme 1. A typical schematic representation for the formation of Ag@mTiO$_2$ hierarchical nanostructures.

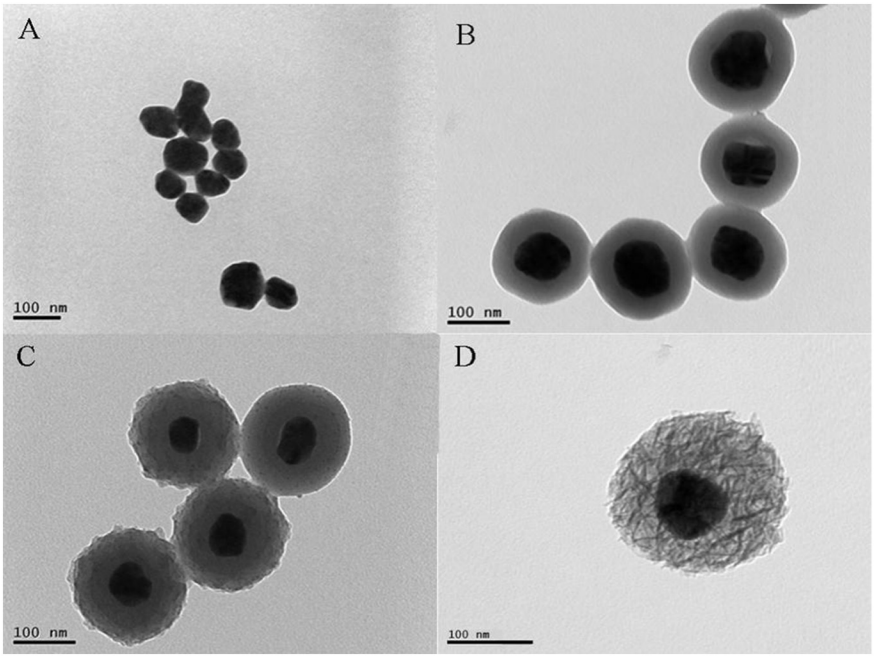

Fig. 1. TEM images of various products: (A) Ag NPs, (B) Ag@SiO_2 with the SiO_2 layer of 30 nm, (C) Ag@SiO_2@TiO_2 with the TiO_2 shell of 30 nm, (D) Ag@mTiO_2 prepared from C. The amounts of TEOS and TBOT used were both 1000 μL, as described in the typical experiment.

In recent years, Ag nanoparticles have fascinating optical properties known as localized surface plasmon resonance (LSPR), which is essential to applications for surface-enhanced Raman scattering (SERS), optical sensing, and bioimaging [42]. Considering that, Rhodamine 6G was used as probe molecule to test the SERS of nest-like Ag@mTiO_2 nanoparticles. Seen from Fig. 3A, the product showed the perfect SERS

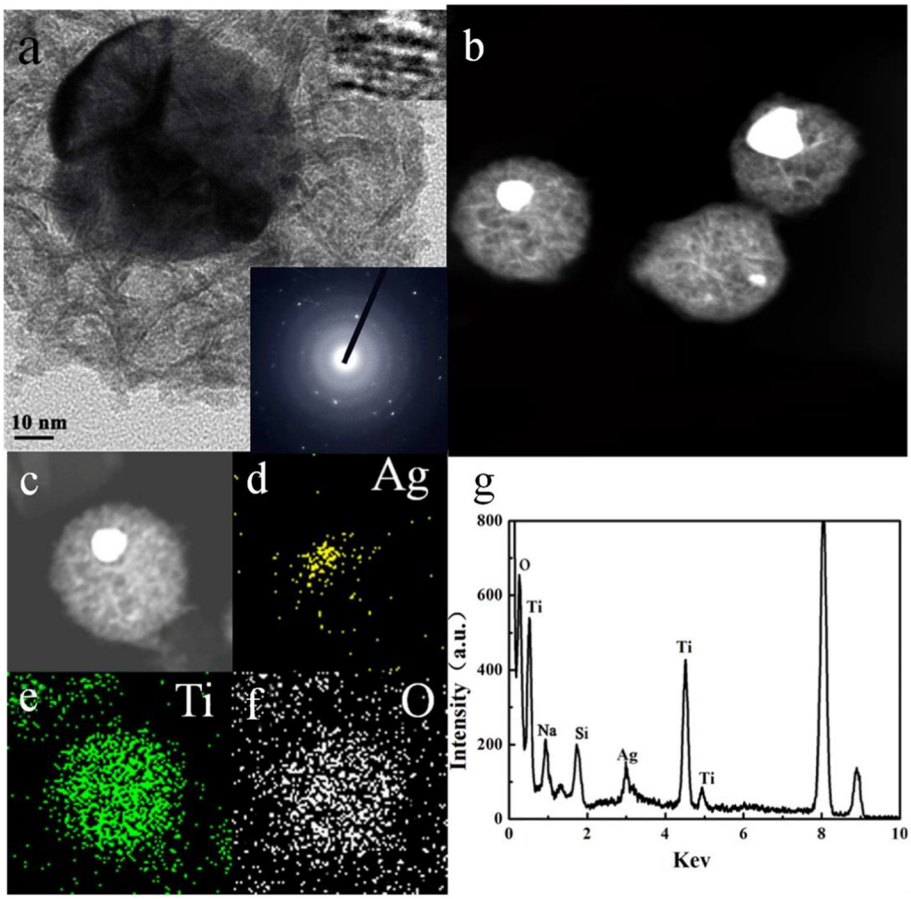

Fig. 2. (a) HRTEM image (inset is the magnified HRTEM image and SAED pattern, respectively), (b, c) STEM images, (d-f) The corresponding elemental maps of Ag, Ti, and O, (g) EDX spectrum of typical nest-like Ag@mTiO_2 nanoparticles.

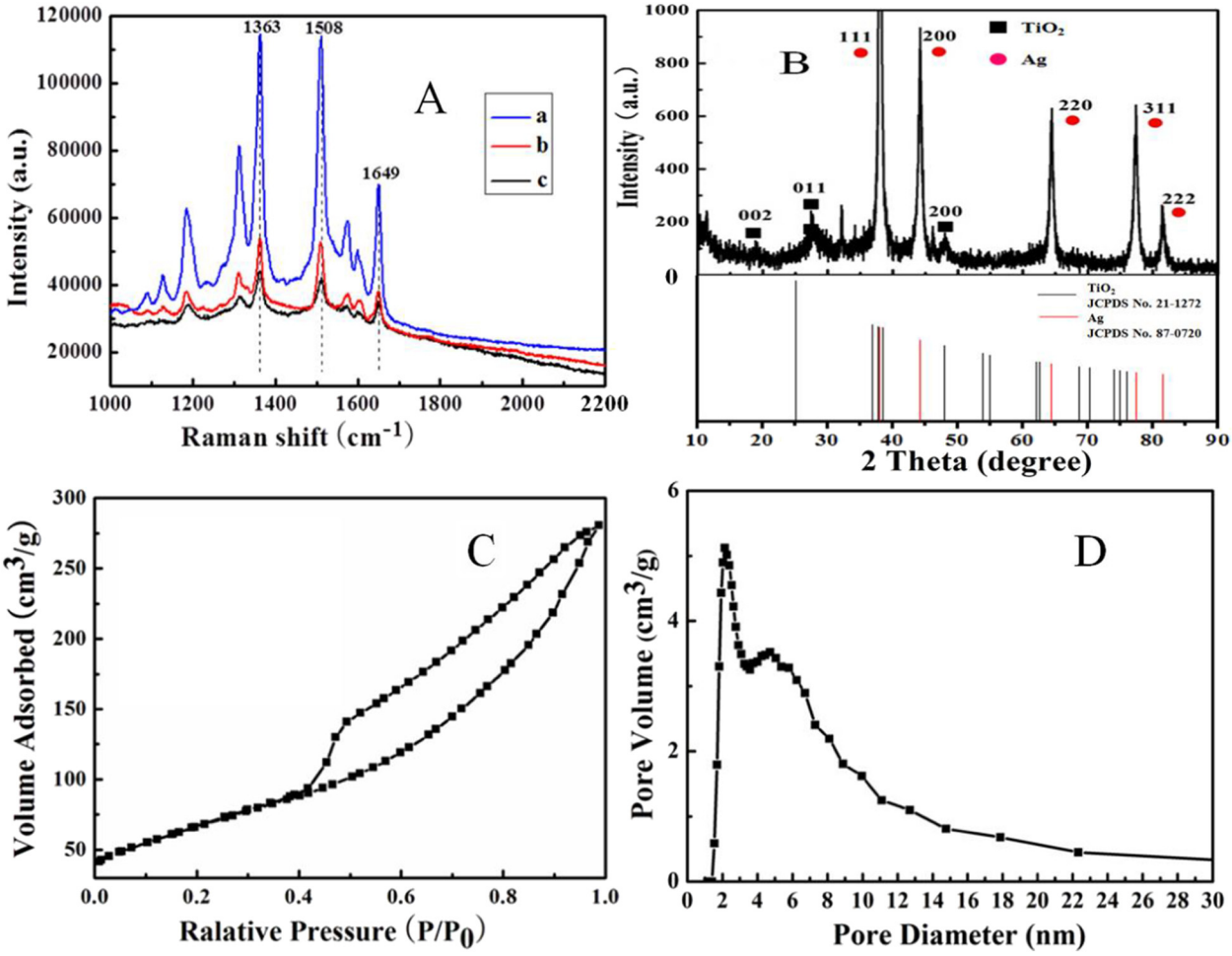

Fig. 3. (A) Raman spectra of Ag nanoparticles (a), Ag@mTiO$_2$ (b), and Ag@mTiO$_2$ nanoparticles placed for a month (c); (B) XRD pattern, (C) N_2 adsorption-desorption isotherm, (D) The corresponding pore size distribution of nest-like Ag@mTiO$_2$ nanoparticles.

signal of the tags enhanced (Fig. 3A). Although the SERS signal of Ag@mTiO$_2$ (Fig. 3A-b) was weaker than Ag NPs (Fig. 3A-a), which was much stronger than that of Ag@SiO$_2$@TiO$_2$ and Ag@SiO$_2$ NPs (Fig. S4). Moreover, Ag@mTiO$_2$ NPs after placing for a month still showed very strong signals (Fig. 3A-c), indicating a good stability, which was ascribed to the protective shell of TiO$_2$. XRD technique was utilized to detect the crystal phase of the products. As shown in Fig. 3B, the resulting Ag@mTiO$_2$ NPs exhibited an obvious Ag crystal phase and a typical anatase TiO$_2$ phase, in which well-resolved diffraction peaks indexed to the (111), (200), (220), (311), and (222) reflections was ascribed to the face-centered cubic Ag (JCPDS card No. 87–0720) with a good crystallinity, compared with pure Ag NPs (Fig. S5). At the same time, the (022), (011), and (200) reflections of a typical anatase TiO$_2$ material (JCPDS card No. 21-1272) were clearly observed, indicating the high crystallinity of TiO$_2$ product. Fig. 3C presented the N_2 adsorption-desorption isotherm of the product. A type-IV curve with a discern hysteresis loop ($P/P_0 > 0.4$) was clearly seen, revealing the existence of mesopores. The product had a high BET surface area of 301 m^2/g and the pore volume was calculated to be 0.47 cm^3/g. The corresponding pore size distribution was in the range of 2–6 nm (Fig. 3D), which was mainly from the aggregation of nanoparticles.

3.2. Potential applications

In practical application, the susceptibility of elemental Ag to oxidation often leads to corner truncation and thus deterioration of SERS activity. The toxicity of the released Ag^+ ions also limits the SERS application of Ag NPs in a biological system. Consequently, before as the drug carrier, we firstly investigated the biocompatibility of Ag@mTiO$_2$ NPs. The cell viability was evaluated by using a cell counting kit-8 (CCK-8) assay. As displayed in Fig. 5, mesenchymal stem cells (MSC) were co-cultured with Ag@mTiO$_2$ NPs at the concentrations in the range of 5–50 mg/mL for 12 h and 24 h, respectively. The CCK-8 results indicated that the cell viabilities (Fig. 4A and B) were above 97%, even higher than 100%, suggesting that the Ag@mTiO$_2$ product had a good biocompatibility. To some degree, the Ag@mTiO$_2$ product also plays the role of cell proliferation, even at the high concentration of 50 μg/mL. Furthermore, the corresponding optical photos of MSC after co-incubation with 50 μg/mL of Ag@mTiO$_2$ for 12 h and 24 h, respectively, were displayed in Fig. 4D and E. Compared with the blank control (Fig. 4C), there was nearly no cell apoptosis and the morphology of the cells still kept well. The good biocompatibility may be due to the protection of TiO$_2$ porous shell, which may be considered as the drug carrier for more biomedical application.

Subsequently, the drug-loading capacity of as-prepared nest-like Ag@mTiO$_2$ NPs was evaluated by using antibacterial drug doxycycline (Doxy) as a model. UV–Vis absorption spectroscopy was used to determine the effective Doxy-storage capacity of the Ag@mTiO$_2$ NPs. As shown in Fig. 5A, the decrease in absorbance at 272 nm was attributed to the integrated effects between the loading concentration and loading capacity. Compared with blank Ag@mTiO$_2$ nanoparticles, the Doxy-loaded Ag@mTiO$_2$ product appeared distinct absorption peaks corresponding to Doxy, indicating the successfully loading of Doxy (Fig. 5B). The loading

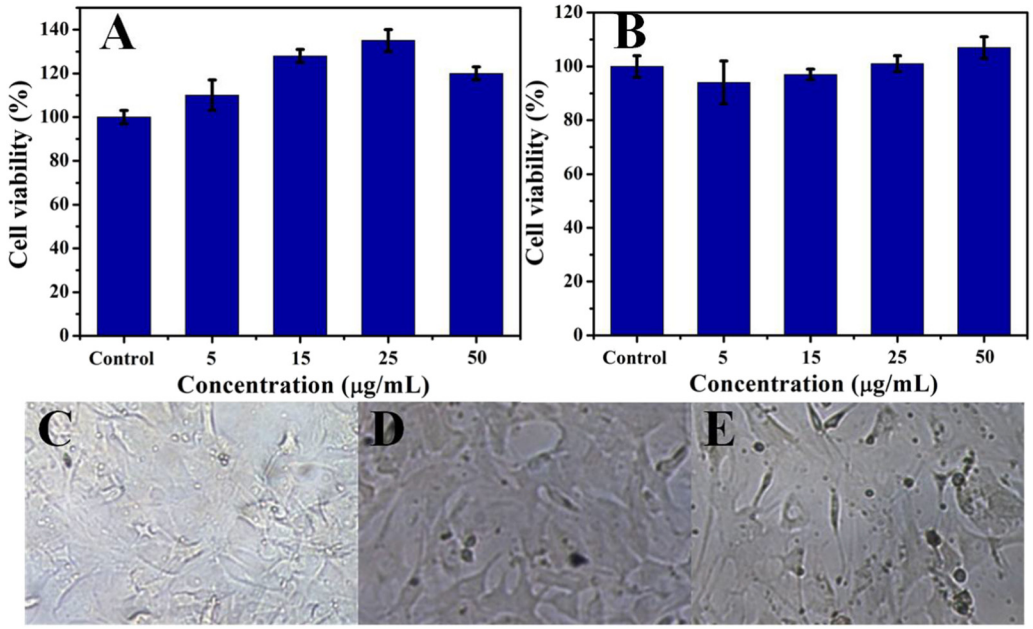

Fig. 4. Cell viability of nest-like Ag@mTiO$_2$ nanoparticles using MSC cultured at different concentrations for 12 h (A) and 24 h (B), optical microscopy of control MSC (C), after co-incubation with 50 μg/mL nest-like Ag@mTiO$_2$ nanoparticles for 12 h (D) and 24 h (E), respectively.

efficiency significantly increased with enhanced Doxy concentrations from 1.0 to 3.5 mg/mL, as shown in Fig. 5C. When the concentration is 1.0 mg/mL, only 27 wt% of Doxy was loaded onto the Ag@mTiO$_2$. Further increasing the concentration to 3.0 mg/mL, about 78 wt% of Doxy could be encapsulated into the Ag@mTiO$_2$. That was slightly lower than 81 wt% of Doxy when the concentration is 3.5 mg/mL. The superior drug-loading

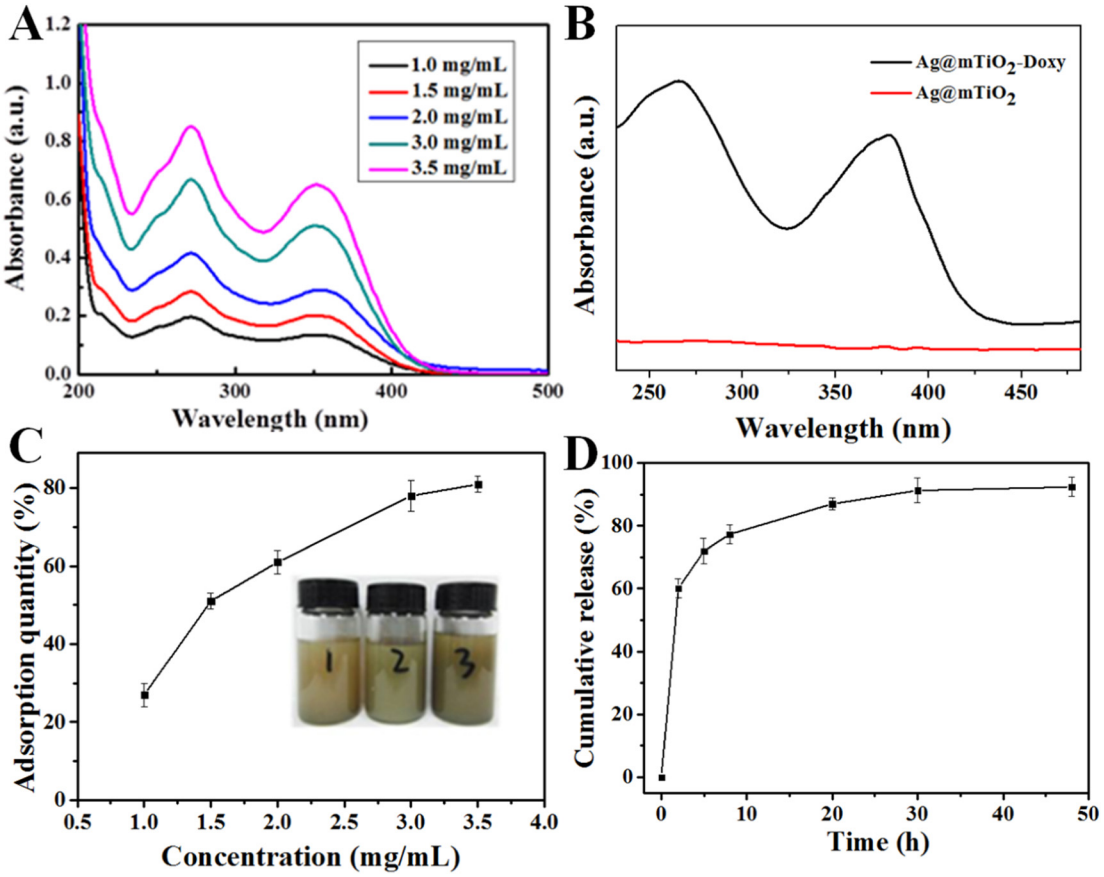

Fig. 5. (A) UV–Vis absorption spectra of Doxy molecules for separated supernatant solutions with different loading concentrations, (B) UV–Vis absorption spectra of Ag@mTiO$_2$ before and after loading of Doxy, (C) The loading efficiency of Ag@mTiO$_2$ with different concentrations of Doxy (Inset is the digital photos of Ag@mTiO$_2$ solutions after loading different Doxy amounts including 1, 2, and 3 mg/mL), (D) The release profile of Doxy-loaded Ag@mTiO$_2$ at PBS solution (pH = 7.4).

capacity of Ag@mTiO_2 NPs is higher than the reported materials [43,44]. That may be mainly attributed to their large surface area and porous TiO_2 shell assembled with nanosheets, which could provide more room for drug molecule. Moreover, the discrepancy of loading capacity was directly observed according to the color change of the precipitate from pale yellow (1.0 mg/mL) to brown (3.0 mg/mL) after absorbing Doxy (inset in the Fig. 5C). Meanwhile, the release behaviour of Doxy-loaded Ag@mTiO_2 (3.0 mg/mL) was also studied in PBS (pH = 7.4) solution. As can be seen from Fig. 5D, Doxy underwent a fast releasing process in the initial 8 h, where above 75 wt% of Doxy was released in this period. After 48 h, about 92 wt% of Doxy was released. After that, the release amount of Doxy had no obvious increase, suggesting an equilibrium release period had been achieved. Overall, the prepared Ag@mTiO_2 NPs exhibited a high drug-loading capacity and excellent release properties.

4. Conclusions

In summary, we have successfully fabricated the Ag@mTiO_2 hierarchical nanoparticles with high specific surface area and uniform morphology by an alkali-etching hydrothermal assisted crystallization method. The characterization results indicated that the thickness of TiO_2 shell layer played a critical role for the formation of the final nest-like unique nanostructure. At the same time, the coated silica layer was used both as medium and template. By simply changing the hydrothermal reaction conditions, the desired structure can be obtained. More importantly, the porous composites prepared exhibited excellent properties such as high drug loading capacity, strong SERS and good biocompatibility. The study has important implications for preparation of other core-shell porous nanomaterials. We also believe that the Ag@mTiO_2 with unique nanostructure will serve as ideal candidates for more potential applications in targeted drug release, photocatalysis, and biosensor, etc.

Acknowledgments

The authors appreciate the financial support provided by the National Natural Science Foundation of China (21471096, 11275121), and Program for Innovative Research Team in University (IRT13078).

Appendix A. Supplementary data

Supplementary data to this article can be found online at http://dx.doi.org/10.1016/j.msec.2017.03.018.

References

[1] C.T. Kresge, M.E. Leonowicz, W.J. Roth, J.C. Vartuli, J.S. Beck, Ordered mesoporous molecular sieves synthesized by a liquid-crystal template mechanism, Nature 359 (1992) 710–712.
[2] H.J. Lee, S.E. Kim, I.K. Kwon, C. Park, C. Kim, J. Yang, S.C. Lee, Spatially mineralized self-assembled polymeric nanocarriers with enhanced robustness and controlled drug-releasing property, Chem. Commun. 46 (2010) 377–379.
[3] N.G. Liu, D.R. Dunphy, P. Atanassov, S.D. Bunge, Z. Chen, G.P. López, T.J. Boyle, C.J. Brinker, Photoregulation of mass transport through a photoresponsive azobenzene-modified nanoporous membrane, Nano Lett. 4 (2004) 551–554.
[4] F. Torney, B.G. Trewyn, V.S.Y. Lin, K. Wang, Mesoporous silica nanoparticles deliver DNA and chemicals into plants, Nat. Nanotechnol. 2 (2007) 295–300.
[5] H.J. Zhang, Z.Y. Li, P.P. Xu, R.F. Wu, Z. Jiao, A facile two-step synthesis of novel chrysanthemum-like mesoporous silica nanoparticles for controlled pyrene release, Chem. Commun. 46 (2010) 6783–6785.
[6] J. Kim, J.E. Lee, J. Lee, J.H. Yu, B.C. Kim, K. An, Y.H. Wang, C.H. Shin, J.G. Park, J. Kim, T. Hyeon, Magnetic fluorescent delivery vehicle using uniform mesoporous silica spheres embedded with monodisperse magnetic and semiconductor nanocrystals, J. Am. Chem. Soc. 128 (2006) 688–689.
[7] L. Zhang, S.Z. Qiao, Y.G. Jin, H.G. Yang, S. Budihartono, F. Stahr, Z.F. Yan, X.L. Wang, Z.P. Hao, G.Q. Lu, Fabrication and size-selective bioseparation of magnetic silica nanospheres with highly ordered periodic mesostructure, Adv. Funct. Mater. 18 (2008) 3203–3212.
[8] J. Liu, S.Z. Qiao, Q.H. Hu, G.Q. Lu, Magnetic nanocomposites with mesoporous structures: synthesis and applications, Small 7 (2011) 425–443.
[9] P. Botella, A. Corma, M.T. Navarro, M. Quesada, Design of optically active nanoclusters of gold particles with mesostructured silica coating, J. Mater. Chem. 19 (2009) 3168–3175.
[10] Y.S. Lin, C.L. Haynes, Synthesis and characterization of biocompatible and size-tunable multifunctional porous silica nanoparticles, J. Chem. Mater. 21 (2009) 3979–3986.
[11] X.F. Zhang, L. Clime, H. Roberge, F. Normandin, L. Yahia, E. Sacher, T. Veres, pH-triggered doxorubicin delivery based on hollow nanoporous silica nanoparticles with free-standing superparamagnetic Fe_3O_4 cores, J. Phys. Chem. C 115 (2011) 1436–1443.
[12] Y.H. Deng, D.W. Qi, C.H. Deng, X.M. Zhang, D.Y. Zhao, Superparamagnetic high-magnetization microspheres with an Fe_3O_4@SiO_2 core and perpendicularly aligned mesoporous SiO_2 shell for removal of microcystins, J. Am. Chem. Soc. 130 (2008) 28–29.
[13] Y.H. Deng, Y. Cai, Z.K. Sun, J. Liu, C. Liu, J. Wei, W. Li, C. Liu, Y. Wang, D.Y. Zhao, Multifunctional mesoporous composite microspheres with well-designed nanostructure: a highly integrated catalyst system, J. Am. Chem. Soc. 132 (2010) 8466–8473.
[14] D.H. Wang, Z. Jiao, M.H. Wu, L.B. Gu, Z.W. Chen, H.J. Zhang, A simple, rapid, one-step approach for preparation of Ag@TiO2 nanospheres with multiple cores as effective catalyst, RSC Adv. 6 (2016) 99878–99884.
[15] Y. Chen, H.R. Chen, S.J. Zhang, F. Chen, L.X. Zhang, J.M. Zhang, M. Zhu, H.X. Wu, L.M. Guo, J.W. Feng, J.L. Shi, Multifunctional mesoporous nanoellipsoids for biological bimodal imaging and magnetically targeted delivery of anticancer drugs, Adv. Funct. Mater. 21 (2011) 270–278.
[16] H.J. Zhang, G.D. Du, W.Q. Lu, L.L. Cheng, X.D. Zhu, Z. Jiao, Porous TiO_2 hollow nanospheres: synthesis, characterization and enhanced photocatalytic properties, CrystEngComm 14 (2012) 3793–3801.
[17] R. Guo, L. Zhang, H. Qian, R. Li, X. Jiang, B. Liu, Multifunctional nanocarriers for cell imaging, drug delivery, and near-IR photothermal therapy, Langmuir 26 (2010) 5428–5434.
[18] X. Li, J. Guo, J. Asong, M.A. Wolfert, G.J. Boons, Multifunctional surface modification of gold-stabilized nanoparticles by bioorthogonal reactions, J. Am. Chem. Soc. 133 (2011) 11147–11153.
[19] P.F. Jiao, H.Y. Zhou, L.X. Chen, B. Yan, Cancer-targeting multifunctionalized Goldnanoparticles in imaging and therapy, Curr. Med. Chem. 18 (2011) 2086–2102.
[20] Y. Guo, D.L. Shi, H.S. Cho, Z.Y. Dong, A. Kulkarni, G.M. Pau-letti, W. Wang, J. Lian, W. Liu, L. Ren, Q.Q. Zhang, G.K. Liu, C. Huth, L.M. Wang, R.C. Ewing, In vivo imaging and drug storage by quantum-dot-conjugated carbon nanotubes, Adv. Funct. Mater. 18 (2008) 2489–2497.
[21] S.H. Hu, K.T. Kuo, W.L. Tung, D.M. Liu, S.Y. Chen, A multifunctional nanodevice capable of imaging, magnetically controlling, and in situ monitoring drug release, Adv. Funct. Mater. 19 (2009) 3396–3403.
[22] J. Kim, H.S. Kim, N. Lee, T. Kim, H. Kim, T. Yu, I.C. Song, W.K. Moon, T. Hyeon, Multifunctional uniform nanoparticles composed of a magnetite nanocrystal core and a mesoporous silica shell for magnetic resonance and fluorescence imaging and for drug delivery, Angew. Chem. Int. Ed. 47 (2008) 8438–8441.
[23] X.J. Wu, D.S. Xu, Soft template synthesis of yolk/silica shell particles, Adv. Mater. 22 (2010) 1516–1520.
[24] Y.Q. Wang, L.X. Chen, P. Liu, Biocompatible triplex Ag@SiO_2@mTiO_2 core-shell nanoparticles for simultaneous fluorescence-SERS bimodal imaging and drug delivery, Chem. Eur. J. 18 (2012) 5935–5943.
[25] S.H. Liu, M.Y. Han, Silica-coated metal nanoparticles, Chem. Asian. J. 5 (2010) 36–45.
[26] Z.W. Seh, S.H. Liu, S.Y. Zhang, K.W. Shah, M.Y. Han, Synthesis and multiple reuse of eccentric Au@TiO_2 nanostructures as catalysts, Chem. Commun. 47 (2011) 6689–6691.
[27] Y.Z. Piao, H.S. Kim, Y.E. Sung, T. Hyeon, Facile scalable synthesis of magnetite nanocrystals embedded in carbon matrix as superior anode materials for lithium-ion batteries, Chem. Commun. 46 (2010) 118–120.
[28] A. Guerrero-Martinez, J. Perez-Juste, L.M. Liz-Marzan, Recent progress on silica coating of nanoparticles and related nanomaterials, Adv. Mater. 22 (2010) 1182–1195.
[29] J.C. Park, H. Song, Metal@silica yolk-shell nanostructures as versatile bifunctional nanocatalysts, Nano Res. 4 (2011) 33–49.
[30] J.P. Yang, F. Zhang, Y.R. Chen, S. Qian, P. Hu, W. Li, Y.H. Deng, Y. Fang, L. Han, M. Luqman, D.Y. Zhao, Core-shell Ag@SiO_2@mSiO_2 mesoporous nanocarriers for metal-enhanced fluorescence, Chem. Commun. 47 (2011) 11618–11620.
[31] L.F. Tan, D. Chen, H.Y. Liu, F.Q. Tang, A silica nanorattle with a mesoporous shell: an ideal nanoreactor for the preparation of tunable gold cores, Adv. Mater. 22 (2010) 4885–4889.
[32] Y. Chen, H.R. Chen, L.M. Guo, Q.J. He, F. Chen, J. Zhou, J.W. Feng, J.L. Shi, Hollow/rattle-type mesoporous nanostructures by a structural difference-based selective etching strategy, ACS Nano 4 (2010) 529–539.
[33] J.H. Gao, G.L. Liang, B. Zhang, Y. Kuang, X. Zhang, B. Xu, FePt@CoS_2 yolk-shell nanocrystals as a potent agent to kill HeLa cells, J. Am. Chem. Soc. 129 (2007) 1428–1433.
[34] H.X. Li, H.X. Bian, Z.F. Zhu, J. Zhang, D.Q. Li, G.S. Huo, Y.N. Li, Y.F. Lu, Mesoporous titania spheres with tunable chamber structure and enhanced photocatalytic activity, J. Am. Chem. Soc. 129 (2007) 8406–8407.
[35] G.L. Li, Q. Shi, S.J. Yuan, K.G. Neoh, E.T. Kang, X.L. Yang, Alternating silica/polymer multilayer hybrid microspheres templates for double-shelled polymer and inorganic hollow microstructures, J. Chem. Mater. 22 (2010) 1309–1317.
[36] X.J. Wu, D.S. Xu, Formation of yolk/SiO_2 shell structures using surfactant mixtures as template, J. Am. Chem. Soc. 131 (2009) 2774–2775.
[37] W. Li, Y.H. Deng, Z.X. Wu, X.F. Qian, J.P. Yang, Y. Wang, D. Gu, F. Zhang, B. Tu, D.Y. Zhao, Hydrothermal etching assisted crystallization: a facile route to functional yolk-shell titanate microspheres with ultrathin nanosheets-assembled double shells, J. Am. Chem. Soc. 133 (2011) 15830–15833.

[38] Y.Q. Wang, G.Q. Hu, X.F. Duan, H.L. Sun, Q.K. Xue, Microstructure and formation mechanism of titanium dioxide nanotubes, Chem. Phys. Lett. 365 (2002) 427–431.
[39] Z.Y. Yuan, J.F. Colomer, B.L. Su, Titanium oxide nanoribbons, Chem. Phys. Lett. 363 (2002) 362–366.
[40] A.G. Martinez, J.P. Juste, L.M. Marzan, Recent progress on silica coating of nanoparticles and related nanomaterials, Adv. Mater. 22 (2010) 1182–1195.
[41] Y.G. Sun, Y.N. Xia, Mechanistic study on the replacement reaction between silver nanostructures and chloroauric acid in aqueous medium, J. Am. Chem. Soc. 126 (2004) 3892–3901.
[42] T. Hirakawa, P.V. Kamat, Charge separation and catalytic activity of Ag@TiO_2 core-shell composite clusters under UV-irradiation, J. Am. Chem. Soc. 127 (2005) 3928–3934.
[43] M.H. Alkhraisat, C. Rueda, J.C. Azama, J.L. Aparicio, F.T. Mariño, J.T.G. Denche, B. Jerez, U. Gbureck, E.L. Cabarcos, Loading and release of doxycycline hyclate from strontium-substituted calcium phosphate cement, Acta Biomater. 6 (2010) 1522–1528.
[44] T. Dedova, M. Krunks, O. Acik, D. Klauson, O. Volobujeva, A. Mere, Hierarchical nanostructures of ZnO obtained by spray pyrolysis, Mater. Chem. Phys. 141 (2013) 69–75.